A Macroanalysis of Hsdpa Receiver Models

Ahmet Başтuğ
Philips Semiconductors
06560, Sophia Antipolis, FRANCE
tel: 33-492944130 fax: 33-492961280
ahmet.bastug@philips.com

Dirk T.M. Slock
Eurecom Institute
06904, Sophia Antipolis, FRANCE
tel: 33-493002606 fax: 33-493002627
slock@eurecom.fr

***Abstract*— We consider high speed packet data access service (HSDPA) which is introduced with the Release-5 of UMTS-FDD standard. Signal to interference + noise ratio (SINR) and throughput bounds from the usage of channel matched filter (RAKE in FIR form) and LMMSE equalizer + correlator type mobile terminal receiver structures are obtained for the high speed downlink shared channels (HSDSCHs) under certain residual intracell interference levels which represent the situations after the possible usage of front end intracell interference cancellers. Exact orthogonality factor expression is obtained which is valid for any type of linear receiver. The distributions of radio channel parameters and received powers from the own and surrounding base stations are modeled under correlated shadowing w.r.t the mobile position, the cell radius and the type of environment. From such modeling, more realistic performance figures might be obtained as compared to fixing them to certain values.**

I. INTRODUCTION

At the time of Cannes 3GSM Congress in 2004, operators celebrated reaching to 1 billion GSM users. Providing a huge market for the EDA vendors, hardware/software manufacturers, operators and service/application providers, further success of the cellular business depends on both supporting much more speech connections (first priority and the highest revenue source for today) and providing higher-rate data applications than before. Currently deployed 2G GSM networks and the 2.5G patches constructed on them like GPRS, EDGE, i-mode satisfy these demands to a certain extent. Speech being a less concern, though limiting the rest available cell capacity, data service rates go up to 384kbps with these 2.5G technologies in realistic scenarios. Even though in a good scenario (a static or a line-of-sight (LOS) condition) the 3G UMTS technology supports up to 2Mbps, this might even not be sufficient for the demands of high-end data-hungry applications. Especially corporate customers are quite interested with obtaining much higher rates, desiring the same capability from a laptop on the move out of office as they get from a workstation in the office. Video games, mp3s, mpegs constitute another huge commercial potential. With further threat from competing/complementary air access technologies such as Bluetooth, IEEE 802.16, WI-FI, HIPERLAN, IEEE802.11a claiming to go upto 54mbps, 3G UMTS work groups had to do something to improve the supported data rate: High Speed Packet Data Access (HSDPA), so called 3.5G claiming to go upto 11Mbps [1], [2].

In this study, our aim within the context of HSDPA is to have broad estimates of the gains by using more developed receivers w.r.t the conventional CMF (FIR form of Rake). This is extremely important since unlike for dedicated channels (DCHs) where a better performing mobile receiver serves only for the benefit of the base station, for HSDSCHs, a mobile terminal *directly benefits* from having an advanced receiver by obtaining more data rate once the connection is established and by increasing the chance of getting a connection if fairness is partially sacrificed for capacity in user scheduling.

The paper is organized as follows: Section II is a brief overview of HSDPA. In section III, after covering the system model, we discuss last stage linear FIR filter receivers at mobile terminals and give our interpretation of the so-called orthogonality factor in their context. In section IV, we outline the modeling of some radio link performance measures like received powers from the own and surrounding BSs, rms delay spread, power delay profile and channel parameters. Last section is devoted to simulation results and comments.

II. HSDPA OVERVIEW

A cellular multi-acces system has certain requirements to satisfy the most important of which are providing enough capacity, coverage and a variety of services each with different QoS and rate requirements. The first two are conflicting: Increasing the coverage area of cells, that is decreasing the number of deployed base stations, decreases the system capacity. In other words, any advanced receiver or transmission diversity technique that normally focuses on improving the spectral efficiency of the system might instead or at the same time be exploited for increasing the coverage. At the launch of a new WCDMA network, operator's first priority will be covering a large area, giving mostly speech and low-rate data services. However, once full coverage is achieved, capacity becomes an immediate concern triggered mostly by high rate data-service requirements. In the UMTS standard, four QoS classes are defined with differing delay and ordering needs [3]:

1. Conversational: low delay, strict ordering, e.g: voice
2. Streaming: modest delay, strict ordering, e.g: video
3. Interactive: modest delay, modest ordering, e.g: web browsing
4. Background: no delay guarantee, no ordering, e.g: bulk data transfer

Among these classes, background and interactive have a bursty nature. This burstiness triggered the idea of user time sharing of some of the resources, most importantly the orthogonal codes in the downlink, along with other supporting techniques, extensions, changes, removals applied on these channels. Hence, HSDPA emerged with following properties:

1. Allocation of multiple acess codes for HSDPA service: To exploit the data burstiness for spectral efficiency and increased link adaptation dynamic range, 1 up to 15 of the 16 orthogonal code resources at spreading factor (SF) 16 are allocated as high speed downlink shared channels (HS-DSCHs) and dynamically time multiplexed among demanding users.

2. Fast scheduling of allocated codes: The goal is to exploit *multiuser diversity*,i.e the temporal channel quality variance among the users, in order to increase the *sum capacity*, that is the total delivered payload by the BS. By one extreme approach, one can assign (preferably) all the codes to a single user with the instantaneously best channel conditions, maximizing the throughput. At the other extreme, users might be served in a *fair* round-robin fashion. Operators are here free to choose any set of schedulers compromising throughput and fairness depending on the predicted channel quality, the cell load and the traffic priority class. In order to reduce the delay in signaling and to better track the channel variations, scheduling is performed at Node-B (i.e BS) which is closer to the air interface than done before at radio network controller (RNC) and its granularity is decreased to 2ms (subframe) from previously 10ms (frame) standard. Soft handover is also replaced by fast *best-signaling-cell* selection which can be interpreted as the *spatial* scheduling complementing the *temporal* scheduling.

3. Link adaptation: Perhaps one of the most important changes which influences almost all the new applied HS-DPA techniques is that practically there is *no fast power control* on HSDSCHs and all the instantaneously remaining *allowed* BS power is shared among HSDSCHs [4]. Therefore instantaneous channel quality (CQ) rapidly varies among users and in time since the received power mainly depends on the path loss exponent of the environment and the user distance from the BS. Hence, by explicit measurement reports from the UE based on the SIR of CPICH (common pilot channel) or by making use of the known transmit power of the power-controlled associated downlink DCH, link adaptation mechanism at Node-B adjusts the number of allocated HSDSCH codes, coding/puncturing rate and the modulation scheme (16 QAM being possible besides QPSK at LOS or high received power conditions) to maximize the throughput. Another difference which reduces the overhead is that only one CRC block is added for one transmission time interval (TTI) of 2ms. Because there is no benefit in knowing which transport blocks are erroneous for when one transport block is erroneous with high probability the others are as well.

4. Hybrid automatic repeat request (HARQ): When transmission entities are identified to be erroneous by a well-known protocol like *selective-repeat* or *stop-and-wait*, fast retransmit request is done from Node-B and combinations of soft information from the original transmission and previous retransmissions are utilized to increase the probability of correct reception. These operations fine-tune the effective code rate, in a way compensating for errors in the channel quality estimates used for link adaptation. The two well known such methods are *chase combining* where weighting of identical retransmissions is done and the *incremental redundancy* where additional parity bits are sent each time.

To support the listed functionalities, two additional type of channels are introduced. In the downlink, one or more shared control channels (HS-SCCHs) broadcast HSDPA channel assigned identities, transport format and H-ARQ process identifier. In the uplink, the high speed dedicated physical control channel (HS-DPCCH) carries the status reports for HARQ and the channel quality indicators (CQIs).

For a more complete coverage of HSDPA, see [1], [2], [5], [6].

III. Physical Layer Model and Linear FIR Filters as Last Stages of the Receiver

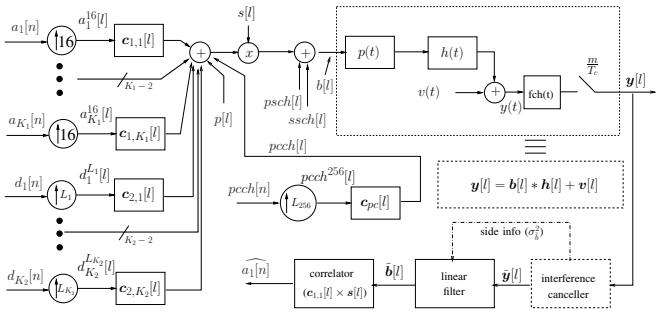

Fig. 1. Baseband downlink transmission and reception model

The baseband downlink model of a UMTS-FDD mode system with HSDPA support is given in Fig. 1. K_1 HSDSCH codes ($c_{1,j}[l], j \in \{1,\ldots,K_1\}; 1 \leq K_1 \leq 15$) are allocated at SF=16 for the transmission of linearly modulated $a_j[n]$ HSDPA symbols of user of interest. $d_j[n], j \in \{1,\ldots,K_2\}$ represent the symbols of possibly existing multi-rate downlink channels like dedicated channels (DCHs), HSSCHs and others except the primary common control physical channel (PC-CPCH), primary common pilot channel (PCIPCH), primary and secondary synchronization channels (PSCH and SSCH) whose chip sequences are demonstrated as $pcch[l]$, $p[l]$, $psch[l]$ and $ssch[l]$ respectively in Fig. 1. At the base station (BS) transmitter, symbols to be carried on a certain channel are first upsampled ($\uparrow$ operator) by their SF and convolved with the corresponding unit-energy Walsh-Hadamard periodic channelization code before summed up with the chip sequence of other channels and multiplied by the unit magnitude BS-specific aperiodic scrambling code $s[l]$. PSCH and SSCH are exceptions, multiplexed late after the scrambler, since as a first-step task in the reception, they are actually utilized for determining the scrambling sequence of the BS. The resultant discrete-time chip sequence $b[l]$ passes through the continuous

transmission channel which is the overall convolution of the root-raised-cosine pulse shape filter $p(t)$ with roll-off factor 0.22 (RRC-0.22), the propagation channel $h(t)$ and the front-end filter $fch(t)$. In the model, the $v(t)$, representing the sum of intercell interference from surrounding base stations and the thermal noise, is added to the BS-originating signal just before the front-end filtering. Furthermore, we assume that there is no beamforming; hence all the chip sequences originating from the same BS pass also through the same propagation channel. We seperated PCIPCH, PCCPCH, PSCH and SSCH since their channelization codes are, like those of the HSDSCH codes, known by the mobile station (MS) and hence an interference canceller (IC) might consider deleting their contribution. On average they consume 10%, 5%, 6% and 4% of the BS power with respectively 100%, 90%, 10% and 10% activity. Hence effectively they eat up 15% of BS power, the majority of which (%65) is consumed by the pilot tone alone [5].

After sampling, the overall continuous time transmission channel can be interpreted as discrete multi-channels by the mobile receiver if the signal is captured by q sensors and sampled at an integer multiple m of the chip rate, rendering the total number of samples per chip $mq > 1$. Stacking these mq samples in vectors, we get the chip rate sampled received vector signal as

$$\boldsymbol{y}[l] = \sum_{i=0}^{N-1} \boldsymbol{h}[i]b[l-i] + \boldsymbol{v}[l] \text{ where,} \tag{1}$$

$$\boldsymbol{y}[l] = \left[\ y_1[l] \dots y_{mq}[l]\ \right]^T, \tag{2}$$

$$\boldsymbol{h}[l] = \left[\ h_1[l] \dots h_{mq}[l]\ \right]^T, \tag{3}$$

$$\boldsymbol{v}[l] = \left[\ v_1[l] \dots v_{mq}[l]\ \right]^T. \tag{4}$$

Here, with a slight abuse of notation, $\boldsymbol{h}[l]$ represents the vectorized samples (represented at chip rate) of the overall channel (assumed to have the same delay spread of N chips) including the pulse shape, the propagation channel and the fch filter. In case of oversampling, fch must be a low pass filter (LPF) with one sided BW equal to half sampling rate to preserve the whiteness of the additive white gaussian noise (AWGN). At chip rate sampling however, fch should be the pulse shape matched filter in order to satisfy the Nyquist criterion. In this paper, we consider $m = 2$ and $q = 1$.

When we model the scramblers as unknown, i.i.d, aperiodic sequences and the symbol sequences as i.i.d., stationary, white sequences, then the chip sequence $b[l]$ is also stationary and white. Therefore, both the intracell and intercell contributions to $\boldsymbol{y}[l]$ are vector stationary processes the continuous-time counterparts of which are cyclostationary with chip period. Finally, the thermal noise also assumed to be white and stationary, $\boldsymbol{y}[l]$ is vector stationary, making chip rate Wiener filtering feasible.

We consider that possibly an IC structure is used in the first discrete-time stage to cancel out one or both of the intracell interference contributions of the pilot tone and HSDPA channels for we know their channelization codes and the symbol constellations (even the symbol values for the pilot tone). To efficiently realize this one can make use of polynomial expansion (PE) type ICs which are constructed from linear minimum mean square error (LMMSE) chip rate equalizers and nonlinear MMSE symbol estimators [7]. Keeping in mind that, in a multirate system, a high-rate user transmission can be equally represented by a number of lower rate users under the root of its orthogonal variable spreading factor (OVSF) code, we can still use robust PE-ICs to blindly cancel other intracell interfering channels whose codes we do not know by linearly deleting out the contributions corresponding to the sufficiently high energy output branches of fast Walsh Hadamard transform (FWHT) at the highest SF (lowest rate) in the system, which in a way implicitly detects the active existence of that highest SF channel or one of its parent channels [7].

After the IC block, we assume that the residual BS signal $\tilde{b}[l]$ contained in the remaining sequence $\tilde{\boldsymbol{y}}[l]$ is still stationary and the second order intercell interference + noise statistics σ_ν^2 is the same as before. So the channel length $(1 \times mN)$ Wiener (LMMSE) filter $\boldsymbol{f}_{mmse}$ that maximizes the SINR for the $\tilde{b}[l]$ by compromising between intracell interference and white noise suppression to minimize the MSE can be defined as

$$\begin{aligned}
&\boldsymbol{f}_{mmse} = \boldsymbol{R}_{\tilde{b}\tilde{y}}\boldsymbol{R}_{\tilde{y}\tilde{y}}^{-1} = \sigma_{\tilde{b}}^2 \boldsymbol{h}^H \boldsymbol{R}_{\tilde{y}\tilde{y}}^{-1} \\
&\boldsymbol{R}_{\tilde{y}\tilde{y}} = E\left[(\boldsymbol{H}\tilde{\boldsymbol{b}} + \boldsymbol{\nu})(\tilde{\boldsymbol{b}}^H \boldsymbol{H}^H + \boldsymbol{\nu}^H)\right] = \sigma_{\tilde{b}}^2 \boldsymbol{H}\boldsymbol{H}^H + \sigma_\nu^2 \boldsymbol{I} \\
&\Rightarrow \boldsymbol{f}_{mmse} = \sigma_{\tilde{b}}^2 \boldsymbol{h}^H (\sigma_{\tilde{\boldsymbol{b}}}^2 \boldsymbol{H}\boldsymbol{H}^H + \sigma_\nu^2 \boldsymbol{I})^{-1} \\
&\Rightarrow \boldsymbol{f}_{unbiased_mmse} = (\boldsymbol{f}_{mmse}\boldsymbol{h})^{-1} \boldsymbol{f}_{mmse}
\end{aligned} \tag{5}$$

where $\boldsymbol{H}$ is the $mN \times 2N-1$ block Toeplitz channel convolution matrix with block size $m \times 1$, $\tilde{\boldsymbol{b}}$ is the residual BS chip sequence of length $2N-1$, $\sigma_{\tilde{b}}^2$ is its variance, $\boldsymbol{R}_{\tilde{y}\tilde{y}}$ is the autocorrelation matrix of the remaining signal and $\boldsymbol{R}_{\tilde{b}\tilde{y}}$ is the cross covariance vector between the remaining signal and the residual BS chip sequence. The purpose of the $\boldsymbol{R}_{\tilde{y}\tilde{y}}$ inversion is to whiten the remaining signal. We observe that when the white noise dominates $\boldsymbol{R}_{\tilde{y}\tilde{y}}$, $\boldsymbol{f}_{unbiased\_mmse}$ becomes the SNR maximizing CMF, $(\boldsymbol{h}^H\boldsymbol{h})^{-1}\boldsymbol{h}^H = \boldsymbol{h}^H$, whereas when the intracell interference dominates, it becomes the SIR maximizing linear minimum mean square error zero forcing equalizer (LMMSE-ZF) bringing back complete orthogonality. Although it is not possible to completely invert an FIR channel by a finite FIR filter, it becomes feasible in case of multichannel setup when there is oversampling or multisensor reception [8].

The chip rate $2N-1$ length now-overall FIR channel $\boldsymbol{g}$ is the m times downsampled convolution of the normalized *unit energy* $\boldsymbol{h}$ and $\boldsymbol{f}$ FIR filters ($\boldsymbol{g} = (\boldsymbol{h} * \boldsymbol{f}) \downarrow m$). The central tap $g(0) = 1$ is the orthogonal useful signal carrying part where the correlator synchronizes and the rest $(g(i), i \in \{-N+1, \dots, -1, 1, \dots N-1\})$ are non-orthogonal interference carrying taps. So the *orthogonality factor* is equal to $\alpha = 1/\|\boldsymbol{g}\|^2$. Note that orthogonality factor is treated in the literature *only* for the Rake receiver variants [9], [10]. However their approaches are approximate in the sense that α is obtained by averaging over the channel (from power delay

profile) and they ignore the correlation between Rake fingers and the effects of the intercell interference+AWGN (in case of G-Rake) whereas our approach is valid for any type of linear filter and *exact*, taking into account the instantaneous channel state.

The signal at the output of the linear filter is downsampled by m and after a delay of N chips, despread by each HSDSCH code of interest (e.g $\boldsymbol{c}_{1,1}[l] \times \boldsymbol{s}[l]$ on Fig. 1) to estimate the HSDPA symbols. The SINR expression for the symbols of a single HSDSCH channel of a MS situated at a certain position of the cell after the despreader block can be written as:

$$SINR = \frac{16\rho P_0}{(1-\alpha)\chi P_0 + \sum_{i=1}^{6} \tilde{P}_i \|\tilde{\boldsymbol{g}}_i\|^2 + \boldsymbol{\nu}_n} \qquad (6)$$

where 16 is the HSDSCH spreading gain, P_0 is the received power of own BS, ρ is the power portion of one HSDSCH channel, χ is the remaining power portion after the IC structure, $\tilde{P}_i$ is the received power from one of first-tier six interfering cells, $\tilde{\boldsymbol{g}}_i$ is the m-times downsampled form of the convolution of the last stage linear filter $\boldsymbol{f}$ and the channel $\tilde{\boldsymbol{h}}_i$ originating from this surrounding cell ($\tilde{\boldsymbol{g}}_i = (\tilde{\boldsymbol{h}}_i * \boldsymbol{f}) \downarrow m$) and $\boldsymbol{\nu}_n$ is the colored (due to $\boldsymbol{f}$) noise variance.

IV. Parameter Modeling

For a single MS, here we model all the parameters making up the SINR expression which implicitly or explicitly depend on one or more of the location of the mobile, the radius (r) of the cell and the environment.

A. Modeling the Received Powers

We express the received power in dBm from a particular BS by large-scale path loss formulation with environment dependant terms as $P_r(dBm) = P_t(dBm) - G_1(dB) - 10nlog_{10}d(dB) + 10log_{10}x(dB)$ where P_t is the transmitted power, G_1 is the path loss at 1km distance, n is the path loss exponent, d is the distance in kilometers and x is the lognormal shadowing term with logarithmic mean 0 and standard deviation σ_x. For shadowing, we first randomly generate a vector of seven independent shadowing values of the own and first-tier six cells and turn it into a cross-correlated vector by left multiplying with the lower triangular Cholesky factorized matrix of the symmetric shadowing corelation matrix whose elements are obtained from the distance proportion and angle values between the corresponding couples among the seven BSs and the mobile position; see [11] for the method and Table 2 therein for the adopted cross-correlation value sets.

B. Modeling the Channel Parameters

The linear filter $\boldsymbol{f}$, the orthogonality factor α and the $\boldsymbol{g}_i$ terms depend on the channel parameters for which we refer to Greenstein's channel model derived from the rms delay spread σ_τ and the power delay profile $P(\tau)$ [12]. Delay spread is equal to $\sigma_\tau = T_1 d^\epsilon y$ where T_1 is the reference delay spread at 1km distance from the BS, ϵ is the model parameter which is around 0.5 for almost all types of environments except very irregular mountainous terrains and y is a coefficient which is lognormally distributed with mean 0 and standard deviation σ_y. From field tests $log(y)$ is also observed to be correlated with $log(x)$ by a factor $\rho_{xy} = -0.75$, [12]. So we first randomly generate a lognormal scalar and modify it by correlating with the obtained shadowing value in the previous section with the same Cholesky factorization technique.

From the obtained delay spread we generate the power delay profile as $P(\tau) \propto e^{-\tau/\sigma_\tau}$ where $\propto$ is the proportionality sign and τ values are the sampling instants. Since this is an infinite length sequence, we truncate it at the position where the final significant tap has $15dB$ less power than the first tap. Then we pass the discrete power delay profile through Rayleigh fading to generate the *propagation* channel. The *transmission* channels are obtained by convolving the obtained propagation channels with the pulse shape and normalizing the result to unit energy.

C. Modeling χ

As explained before, among the common downlink channels, the pilot tone (CPICH) has the highest interference with 10% BS power portion and it can be cancelled with high accuracy [13]. However it might be even more meaningful to consider cancelling the interference of HSDSCH multicodes since by a highly probable deployment scenario, they will carry the majority (if not all) of the data traffic. We contemplate this because it would be easier to manage for an operator to dedicate one of its two or three carriers to HSDPA service instead of distributing it over two or three available carriers. Furthermore there is no justified advantage of carrying high-rate data on multi-rate DCHs instead of multicode HSDPA channels. So, in the reception chain for a single HSDSCH, we define five *perfect* first stage interference cancellation (IC) scenarios:

1. No interference canceller exists: $\chi = 1$
2. Pilot tone cancelled: $\chi = 0.9$
3. All the other HSDSCHs cancelled: $\chi = 1 - (K_1 - 1)\rho$
4. Pilot+HSDSCHs cancelled: $\chi = 0.9 - (K_1 - 1)\rho$
5. All intracell interference cancelled: $\chi = \rho$

V. Simulations and Conclusions

Five different environments are considered, the relevant parameters of which are shown in Table I which are adopted from COST231 propagation models [14] and from [12]. We uniformly position 10^4 MSs in the own cell and approximately that much more in an expanded region penetrating into other cells considering the effect of shadowing handing off some MSs to not-closest BSs. We also exclude a few closest points to the BS since they would otherwise overwhelm all the other MSs. We fix transmitted BS power and AWGN power to $P_t = 43dBm$ and $\boldsymbol{\nu}_n = -102dBm$. For each node receiving the highest power from the BS of interest, we determine the relevant second order statistics and make 10 Rayleigh fading channel realizations. At each realization we obtain the SINR and *bandwidth-normalized* throughput bound $\mathcal{T} = log_2(1 + SINR)$ results for the CMF and LMMSE equalizer-correlator type receivers under five mentioned interference

cancellation scenarios. It was shown that the interference at the output of multiuser detectors can be approximated by Gaussian distribution [15], [16]. Hence $\mathcal{T}$ is an approximate Shannon capacity and it is a more meaningful measure than SINR since it defines the overall performance bound that can be achieved by the usage of efficient transmission diversity, modulation and channel coding schemes. From such around 10^5 spatio-temporal results, we can obtain the distributions of SINR and $\mathcal{T}$. Three different low-end to high-end HSDPA service scenarios are considered with $\{K_1, \rho\}$ sets as $\{1, 0.1\}$,$\{5, 0.06\}$ and $\{10, 0.06\}$.

Cumulative distributions of $\mathcal{T}$ for 10 HSDSCH codes deployment in the five reference environments are shown in Fig. 2 to Fig. 6. The calculated median values of $\mathcal{T}$ for all the defined settings are tabulated in Table II. On the figures and the table, C represents CMF; E represents LMMSE equalizer-correlator receiver; suffixes to C and E ($\{1, \ldots, 5\}$) represent in the same order the IC scenarios defined in section IV-C; {ind, umi, uma, sub} represent {indoor, urban microcell, urban macrocell, suburban macrocell} environments; the suffixes $\{1, 5, 10\}$ to these environments represent K_1.

As observed in the figures, an increasing gap occurs between matched filtering results and equalization results when we go to user locations closer to the own BS which correspond to higher SINR regions. This is especially the valid case for indoor cells, urban microcells and urban macrocells where the eye is open for all user locations since white noise (thermal noise and partially intercell interference) suppressing CMF is much more effected by the intracell interference most of which however is suppressed and the need for an IC decreases when an equalizer is used. In other words, in such environments orthogonality factors at the output of LMMSE equalizers are much higher than those of CMFs. In the suburban macrocell sizes, for the most distant %30 cellular positions, there is no difference in the performance of receivers. When we further go to the extreme rural cell sizes, there is almost no difference except at a small number of very close MS positions. These figures clearly show the dominancy of multiuser interference in small cells where using interference suppressing equalizers becomes meaningful and the dominancy of AWGN in the large cells where CMF or Rake receivers are sufficient. According to UMTS deployment scenarios, more than %80 of UMTS cells will be pico or micro cells and hence it will certainly pay off if a MS considers the LMMSE equalizer in order to be scheduled for a high SINR demanding HSDPA service. In these settings, the achievable *maximum* $\mathcal{T}$ by using equalizers is approximately twice that of CMFs. So, in an ideal condition CMF has less chance of providing a very high rate demanding application.

In Table II, we notice that when an equalizer is used, the median capacity for a MS increases when we move from indoor to urban environments which is mostly because of the trend of path loss exponent, for when it is low, intercell interference will be high. However as we further increase the size of the cell, AWGN starts to dominate and median capacity decreases. We also see that w.r.t CMF, equalizers alone improve the median capacity of pico and micro cells between %60 and %115. When complete interference cancellation is achieved these figures increase to %98 and %199. Cancelling the pilot tone alone brings very little gain. Moshavi et.al however claim that it is possible to obtain %11 capacity gain by cancelling the %10 power pilot tone since this much cancelled power can be exploited by the BS to accept a proportional number of new users [17]. This can be only valid if all the MS receivers at the same time cancel the pilot tone which is not dictated for the moment by the standard. Note that the obtained results are valid when there is no LOS and surrounding cells have identical properties. In reality, we expect higher capacity from picocellular regions since they will be some isolated hot zones like airports and there will be a higher probability of LOS. Furthermore, note that capacity we are here concerned with is the single cell capacity. Of course, global capacity from the adoption of picocells will be much higher than others since there will be more cells and hence more users will be served.

REFERENCES

[1] "3GPP TS 25.848, Physical Layer Aspects of HSDPA, [Online]. Available:http://www.3gpp.org/ftp/Specs."

[2] "3GPP TS 25.855, UTRA High Speed Downlink Packet Access; Overall UTRAN description, [Online]. Available: http://www.3gpp.org/ftp/Specs."

[3] "3GPP TS 23.107, QoS Concept and Architecture, [Online]. Available: http://www.3gpp.org/ftp/Specs."

[4] "3GPP TS 25.214, Physical layer procedures (FDD), [Online]. Available: http://www.3gpp.org/ftp/Specs."

[5] H. Holma and A. Toskala, *WCDMA for UMTS*. John Wiley and Sons, 2000.

[6] P. Frenger, S. Parkvall, and E. Dahlman, "The evolution of wcdma towards higher speed downlink packet data access," *Proc. Vehicular Technology Conference*, Oct 2001.

[7] A. Bastug and D. Slock, "Interference cancelling receivers with global mmse-zf structure and local mmse operations," *Proc.Asilomar Conf. on Signals, Systems & Computers*, November 2003.

[8] C. Papadias and D. Slock, "Fractionally spaced equalization of linear polyphase channels and related blind techniques based on multichannel linear prediction," *IEEE Transactions on Signal Processing, Vol.47, No.3*, March 1999.

[9] K. Pedersen and P. Mogensen, "The downlink orthogonality factors influence on wcdma system performance," *Proc. Vehicular Technology Conference*, September 2002.

[10] N. Mehta, L. Greenstein, T. Willis, and Z. Kostic, "Analysis and results for the orthogonality factor in wcdma downlinks," *Proc. Vehicular Technology Conference*, May 2002.

[11] K. Zayana and B. Guisnet, "Measurements and modelisation of shadowing cross-correlations between two base stations," *Proc. ICUPC, Rome*, October 1998.

[12] L. Greenstein, Y. Yeh, V. Erceg, and M. V. Clark, "A new path gain/delay-spread propagation model for digital cellular channels," *IEEE Transactions on Vehicular Technology, vol.46, no.2*, May 1997.

[13] J. Sadowsky, D. Yellin, S. Moshavi, and Y. Perets, "Cancellation accuracy in cdma pilot interference cancellation," *Proc. Vehicular Technology Conf.*, April 2003.

[14] C. F. Report, "Digital mobile radio towards future generation systems," *COST Telecom Secretariat, European Commission, Brussels, Belgium*, 1999.

[15] J. Zhang, E. Chong, and D. Tse, "Output mai distributions of linear mmse multiuser receivers in ds-cdma systems," *IEEE Transactions on Information Theory, Vol.47, No.3*, March 2001.

[16] H. Poor and S. Verdú, "Probability of error in mmse multiuser detection," *IEEE Transactions on Information Theory, Vol.43, No.3*, May 1997.

[17] J. Sadowsky, D. Yellin, S. Moshavi, and Y. Perets, "Capacity gains from pilot cancellation in cdma networks," *Proc. Wireless Communications and Networking Conf.*, March 2003.

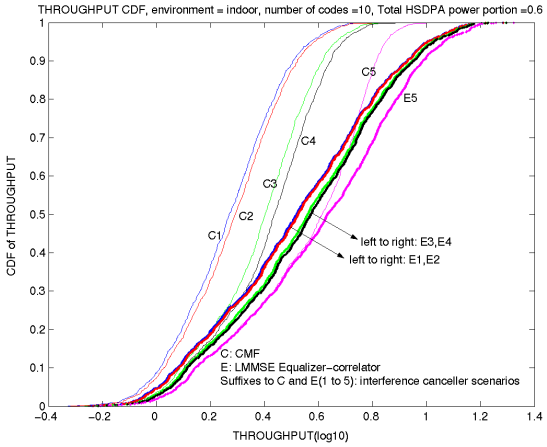

Fig. 2. Throughput bound CDF of indoor microcell

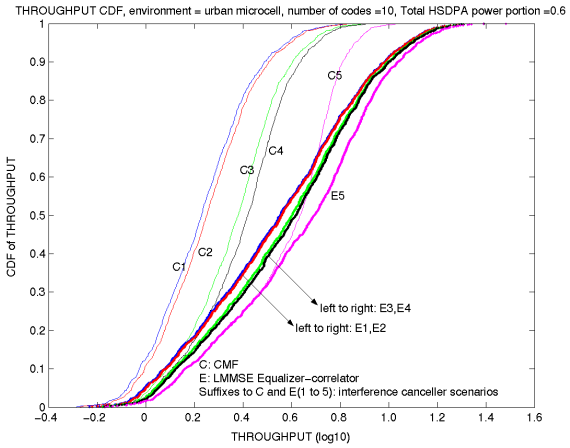

Fig. 3. Throughput bound CDF of urban microcell

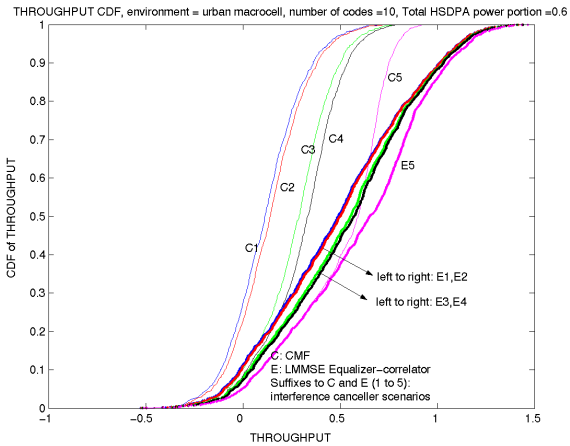

Fig. 4. Throughput bound CDF of urban macrocell

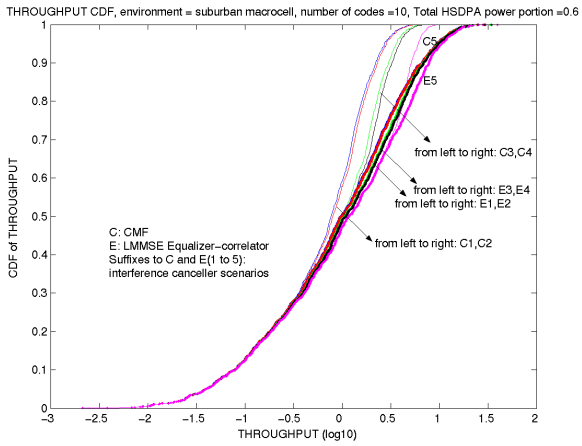

Fig. 5. Throughput bound CDF of suburban macrocell

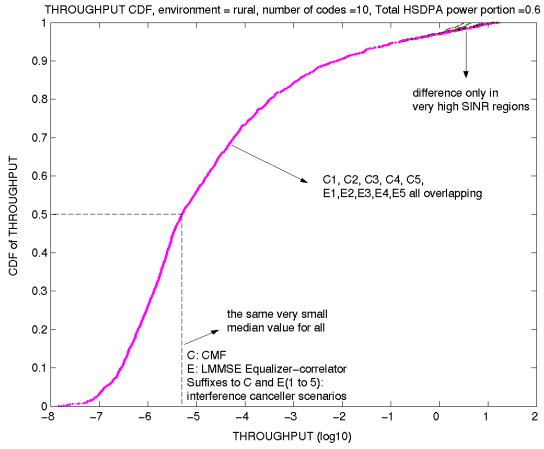

Fig. 6. Throughput bound CDF of rural cell

TABLE I

CELLULAR DEPLOYMENT SCENARIOS

PARAMETERS	G_1	n	r	T_1	σ_x	σ_y
Indoor	138	2.6	0.2	0.4	12	2
Urbanmicro	131	3	0.5	0.4	10	3
Urbanmacro	139.5	3.5	1	0.7	8	4
Suburbanmacro	136.5	3.5	2	0.3	8	5
Rural	136.5	3.85	8	0.1	6	6

TABLE II

THROUGHPUT BOUND MEDIAN RESULTS

$\mathcal{T}$	C1	C2	C3	C4	C5	E1	E2	E3	E4	E5
ind1	2.46	2.54	2.46	2.54	4.54	3.94	3.99	3.94	3.99	4.87
ind5	1.86	1.94	2.09	2.21	4.13	3.22	3.27	3.33	3.42	4.34
ind10	1.86	1.96	2.53	2.73	4.11	3.31	3.35	3.63	3.73	4.30
umi1	2.18	2.29	2.18	2.29	4.54	4.16	4.20	4.16	4.20	5.30
umi5	1.65	1.74	1.89	2.02	4.34	3.56	3.59	3.71	3.77	4.94
umi10	1.70	1.79	2.41	2.63	4.32	3.59	3.63	4.00	4.16	4.95
uma1	1.78	1.88	1.78	1.88	4.13	3.80	3.86	3.80	3.86	5.16
uma5	1.30	1.37	1.50	1.62	3.97	3.09	3.14	3.26	3.35	4.72
uma10	1.30	1.38	1.95	2.15	3.91	3.10	3.17	3.58	3.74	4.50
sub1	1.11	1.17	1.11	1.17	1.60	1.40	1.42	1.40	1.42	1.61
sub5	0.79	0.82	0.87	0.91	1.19	1.02	1.03	1.05	1.06	1.19
sub10	0.77	0.81	0.97	1.02	1.18	0.98	1.00	1.07	1.09	1.18